Modeling transport and filtration of nanoparticle suspensions in porous media

A. ten Bosch*
Centre National de Recherche Scientifique, Parc Valrose, 06108 Nice, France

(Received 18 August 2022; accepted 8 January 2023; published 14 March 2023)

Recently membrane filters have gained in significance due to the need to provide protection against airborne pollution. A question of importance, and some controversy, is the efficiency of filters for small nanoparticles with diameters below 100 nm as these are considered particularly dangerous due to possible penetration into the lungs. The efficiency is measured by the number of particles blocked by the pore structure after passing though the filter. To study the penetration into pores by nanoparticles suspended in a fluid, a stochastic transport theory based on an atomistic model is used to calculate particle density and flow within the pores, resulting pressure gradient, and filter efficiency. The importance of pore size relative to particle diameter and of the parameters of the pore wall interactions are investigated. The theory is applied to aerosols in fibrous filters and found to reproduce common trends in measurements. As particles enter the initially empty pores on relaxation to the steady state the small penetration measured at the onset of filtration increases faster in time the smaller the nanoparticle diameter. Control of pollution by filtration is achieved by strong repulsion of pore walls for particle diameters greater than twice the effective pore width. For smaller nanoparticles the steady-state efficiency decreases as the pore wall interactions weaken. Effective efficiency is increased when the suspended nanoparticles inside the pores combine into clusters of sizes greater than the filter channel width.

DOI: 10.1103/PhysRevE.107.034121

I. INTRODUCTION

Filtering of solid and fluid particles is a field of great importance with applications to waste water treatment, air purification, food processing, pharmaceutical preparation, and many others [1,2]. Various types of porous media are used. The type of material is chosen specifically for a given application and the size of the pores is an important consideration. Virus dimensions are typically in the nanometer range, burning wood from 0.3 to 60 microns and dust particles can range from 1 nm to 10 000 μm. Porous media extend from macroporous wide meshed metallic sieves used to measure and separate solid particles down to the nanometer-size channels of microporous zeolite crystals used in the separation of gases [3]. Paper and cloth based membrane filters [4] have gained in significance due to the need to provide protection against airborne pollution.

To improve existing filters and develop new ones, standardized test methods have been developed to characterize the materials, test their filtering capability and relate structure to filtering efficiency. The experimental setup is described in the review by Wang and Tronville [5] which also provides an overview of filtration test methods and results of recent experimental studies. The basic method is to pass a sample of suspended particles with measured characteristics such as concentration and size distribution through the filter. The difference in the number of particles before and after passing through the filter is determined. The penetration is defined as the ratio of the concentration after passing through the filter (downstream) to the concentration before entering the filter (upstream). The efficiency is then defined as the fraction of particles removed by the filter. Parameters which affect the efficiency are face velocity, aerosol particle size and characteristics of the filter material. Theoretical interpretation is historically based on the ideas of equilibrium Langmuir adsorption and capture of particles by the filter material [6,7]. In the model, flow transports particles sufficiently close to stick to the attractive adsorbing surfaces, by convection and interception in the case of large particles and in the case of small particles, predominantly by diffusion [8]. Efficiency for small nanoparticles with diameters below 0.1 microns is a subject of ongoing research and some controversy due to experimental and theoretical issues for small particle sizes and low concentration [9]. The uncertainty of validity at the nanoscale calls for reconsideration and research into nanoparticle transport by fluids in porous media [10]. Accurate and reliable dynamic models for nanoparticle transport, deposition and aggregation are needed for the development of design tools in a number of technological areas [11,12].

The flow field through pores and the coupling of particle motion to the macroscopic velocity field of air has been examined numerically [13] and a recent review has been published for several model porous structures [14]. Rios de Anda *et al.* [15] used the Boltzmann equation in combination with detailed filter fiber structure to calculate the efficiency from the flux of particles suspended in the flow of the fluid towards the adsorbing surfaces. It was found that efficiency is low as particles smaller than 1.5 μm follow the air through large interyarn pores and exit unimpeded. No quantitative results could be given for the efficiency of filtration by diffusion for particle sizes below 100 nm.

The present calculation is well-adapted to nanosystems. The approach is based on a statistical model for Brownian motion of particles which respond to the erratic force fluctuations of the medium in which they move. The trajectory

*Alexandra.TENBOSCH@univ-cotedazur.fr

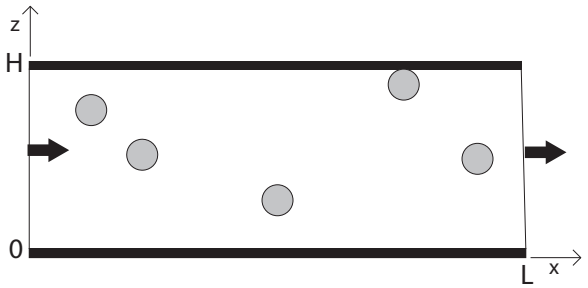

FIG. 1. Schematic representation of the geometry of the slit pore. The number density of suspended particles of diameter σ is held fixed at the pore entrance at $x = 0$ and at the exit at $x = L$. The arrows mark the flow direction in the steady state. The walls of the pore are located at $z = 0$ and $z = H$.

of a Brownian particle follows certain conditions which limit the directional changes of velocity and the average length of a diffusive step. The kinetic theory which is the basis of the present work incorporates such constraints in a path integral formulation to express the statistical probability of a given particle path and to derive the kinetic equation it fulfills [16]. Details of the fluctuating particle paths are suppressed to describe flow patterns that persist for indefinitely long times; by taking appropriate statistical nonequilibrium averages, particle dynamics can be followed from the scale of a single particle on an atomic level to the macroscopic scale of hydrodynamics [17]

The purpose of the present paper is to apply the model to transport of nanoparticles and filtration efficiency in porous media specifically in the lowest range of particle size. The explicit interaction with the pore walls is considered. A filter is selective by the size effect of molecular sieving but also by specific membrane surface interactions. Both these mechanisms break down when the diameters of the particles are much smaller than the pore width. The theory presented in the following predicts low penetration due to the size effect for particle diameters greater than half the pore width. As the particle diameter drops below the critical pore width, penetration increases due to decreasing effect of pore wall interaction.

II. THE MODEL

An analytical solution for the efficiency is possible in the simple model described below (Fig. 1).

A. The particles

Particles suspended in a quiescent fluid such as air enter the channel at $x = 0$ and after passing through the filter exit at $x = L$. The particles are modeled by spheres of diameter σ and mass m. In each pore of the filter particle transport takes place independently. The microparticles studied in this work have diameters of micrometers or less, and the nanoparticle diameters lie below 0.1 μm. The concentration is sufficiently low to consider the particles as independent. The particles can carry a charge distribution but forces are concentrated on the centers of the particles. In a polydisperse sample each particle size permeates independently.

B. The pore structure

Regular pore architecture simplifies theoretical and modeling work and the interpretation of experiments. In the following the theoretical model will concentrate on the effect of the surfaces which form the pores. In a first step to understanding transport in a filter, the phenomena are calculated for a single slit channel with rectangular geometry shown in Fig. 1. The effective channel length along the x axis is L, the width along the z axis is H and $L \gg H$. The walls limiting the channel are located at the top $z = H$ and the bottom $z = 0$ parallel to the xy plane. The surfaces of the channel are assumed to be smooth, surface roughness along the xy planes will not be considered. Each channel of a given size H, L acts independently on the aerosol particles to generate density and velocity profiles which depend on H, L.

The filter medium is a series of channels of different size with pore size distribution function $f(H, L)$. Experimental data measured for the filter are weighted averages in the pore size distribution function of the quantity calculated in the model system. The pore size distribution function can be extracted from other experimental data, assuming the same effective pore structure [18]. To make an analysis possible the actual pore structure is a fit, as here, to a calculation in an idealized model of pore shapes and sizes.

C. The pore wall interaction

Forces from the molecules of the pore surfaces acting on the suspended particles lead to an interplay between fluid transport and the membrane, resulting in rejection or accumulation within the pores of the membrane. Inside the channel the interaction potential $w(z)$ of a single pore surface with the particles is assumed independent of position along the pore length axis. The total interaction $W(z)$ on a particle in the present geometry is the sum of the interactions $w(z)$ from each enclosing surface,

$$W(z) = w(z) + w(H - z). \tag{1}$$

III. CALCULATION

A. Deriving the dynamic equation

The motion of the particles within the channel is described by a set of coupled conservation equations for the local density, the flux, and the pressure. These quantities emerge directly from the kinetic equation derived from the model for the probability distribution as velocity moments of the statistical nonequilibrium distribution in phase space [16].

The zero-order moment is the number density for a given particle size $n(x, z, t)$ which fulfills the equation of continuity (to simplify the notation the variables are not given when obvious). The continuity equation for conservation of particle number is derived as

$$\frac{\partial n}{\partial t} = -\mathrm{div}\vec{j} + D_0 \mathrm{div}[n(\vec{r})\mathrm{grad}(\mu(\vec{r})/kT)]. \tag{2}$$

The diffusion coefficient within the channel D_0 is related to the finite mean free path. The local chemical potential $\mu(x, z)$ in classical density functional theory is applicable to suspensions as well as atomic systems. For low density only the entropy contributes besides the wall interaction [19] and, in

an expansion on the uniform density n_0 and chemical potential μ_0,

$$\mu(x,z) = \mu_0 + kT\ln(n(x,z)/n_0) + W(z). \tag{3}$$

The first-order velocity moment is the flux $\vec{j}$, the number of particles per second and surface area, given by the average velocity of the particles. The flux $\vec{j}$ fulfills the equation for conservation of momentum and for the flux $j_x(x,z,t)$ in the x direction the equation of motion along x is

$$\frac{\partial j_x}{\partial t} = -\beta j_x - \frac{\partial T_{xx}}{\partial x}, \tag{4}$$

Along z the flux in the z direction $j_z(x,z,t)$ fulfills

$$\frac{\partial j_z}{\partial t} = -\beta j_z - \frac{\partial T_{zz}}{\partial z} - T_{zz}\frac{\partial W}{\partial z}. \tag{5}$$

The coefficient β is a measure of the internal friction with the fluid and ensures suppression of large velocity changes with time. The velocity decay time in nanosystems is β^{-1}. The effects of temperature variations for negligible heat conduction, and of viscosity for sufficiently low density are omitted.

The second-order moment is the kinetic energy tensor T_{ij} with relaxation time $(2\beta)^{-1}$. The equation for the kinetic pressure tensor $T_{xx} = T_{zz}$ follows from the equation for conservation of energy

$$\frac{\partial T_{xx}}{\partial t} = -2\beta(T_{xx} - nkT/m). \tag{6}$$

The higher the order of velocity moment the faster the decay to local equilibrium. In an adiabatic description the higher velocity moments decay rapidly to local equilibrium values [20]. After a time $(2\beta)^{-1}$ the pressure tensor at local equilibrium is $T_{xx} = nkT/m$. The flux $\vec{j}(x,z,t)$ will have achieved the local value given by the local driving force,

$$\vec{j}(x,z) = -\frac{kT}{m\beta}n(x,z)\mathrm{grad}(\mu/kT). \tag{7}$$

From Eq. (7) the flux along the channel length is found,

$$j_x = -\frac{kT}{m\beta}\frac{\partial n}{\partial x}, \tag{8}$$

and along the channel width,

$$j_z = -\frac{kT}{m\beta}\left(\frac{\partial n}{\partial z} + n\frac{\partial W/kT}{\partial z}\right). \tag{9}$$

The dynamic aerosol equation [6] is recovered by inserting the flux from Eq. (7) into the continuity equation Eq. (2). The general dynamic equation, GDE, for aerosols is an equation widely used to describe the time evolution of the particle size distribution [21,22]. Further terms can be included such as coagulation (aggregation) and condensation.

The number of particles and their velocity vary with time and position within the pore. After a sufficiently long time a stationary state is established of zero flux in the z direction and steady-state flow along the pore axis. Initial and boundary conditions at the pore entrance and exit are adapted to describe a typical experimental situation. Here, at the pore entrance and exit, the particle density and the chemical potential are held constant thus setting up a pressure gradient. The density at the pore entrance is n_0.

A solution of the dynamic equation is investigated for separation of motion in x along the channel and in z in the perpendicular direction [3] by setting $n(x,z) = n_0 f(x)g(z)$.

B. Solution in the z direction and size effect

The equation in the direction of the pore width is a diffusion equation in the external field created by the pore walls,

$$\frac{\partial g}{\partial t} = D\left[\frac{\partial^2 g}{\partial z^2} + \frac{\partial}{\partial z}\frac{g\partial W(z)}{\partial z}\right]. \tag{10}$$

The effective diffusion coefficient $D = D_0 + kT/m\beta$ is a gauge of the complex pore structure and dependent on particle size. The width of the channel or pore diameter is typically smaller than the channel length. A stationary solution is first established in the z direction in a time of the order of $H^2/\pi^2 D$. The transient profile along the width of the pore decays to the stationary solution. The decay time for example is 10^{-5} s for $H = \mu$m and diffusion constant $D = 10^{-4}$ cm^{2}s^{-1} in air but 1 s for diffusion constant $D = 10^{-9}$ cm^{2}s^{-1} in a dense fiber filter. For $D\pi^2 t/H^2 \gg 1$, the stationary density profile in the z direction is given by

$$g(z) = \exp\left[-\frac{W(z)}{kT}\right], \tag{11}$$

which describes a steady state of vanishing current along z, $j_z = 0$.

C. Solution in the x direction and time effects

The equation along the direction of the pore length is a simple diffusion equation:

$$\frac{\partial f}{\partial t} = D\frac{\partial^2 f}{\partial x^2}. \tag{12}$$

In the x direction the dynamics are purely diffusive. The variations of the surface potential along x are sufficiently small to be neglected. The density at the entrance is held constant so that at the entrance $n(x=0,z,t) = n_0$, and at the exit $n(x=L,z,t) = 0$. The standard solution of the diffusion equation is known for fixed values of density at the boundaries:

$f(x,t) = 1$ at $x = 0$ for equilibrium with the source chamber,

$f(x,t) = 0$ at $x = L$ for equilibrium with the particle-free collection chamber.

The steady state corresponds to a linear profile

$f(x,t) = (1 - x/L)$,

and from Eq. (8) a constant flux along the x direction,

$$j_x = (kT/m\beta L)n_0\exp\left(-\frac{W(z)}{kT}\right). \tag{13}$$

The difference in density at entrance and exit causes a pressure gradient as derived from the Gibbs Duhem equation for local equilibrium, $n\partial\mu/\partial x = \partial p/\partial x$. The pressure drop along the pore channel is $p(L) - p(0) = -n_0 kT$ and the steady-state flux is proportional to the pressure drop through the mobility $1/m\beta$.

The nonstationary solution describes the drift of particles into the empty pore towards the exit. Particles are at

first located close to the pore entrance. For initial condition $n(x, z, t = 0) = 0$, the pore is initially empty of nanoparticles. At $t > 0$ the density is given by

$$f(x,t) = (1 - x/L) - \frac{2}{\pi}\sum_{K=1}\frac{1}{K}\sin(K\pi x/L) \times \exp(-DK^2\pi^2 t/L^2). \quad (14)$$

The characteristic time is $L^2/\pi^2 D$. and the stationary solution of constant flux appears after a time $D\pi^2 t/L^2 > 1$. The decay time for example is 10^4 s for $L = 0.1$ mm and diffusion constant $D = 10^{-9}$ cm^{2}s^{-1} in a dense fiber filter.

At short times, before the steady state is established, the flux at the exit is given by the time dependent Theta function [23] $\theta_4(q = \exp(-D\pi^2 t/L^2, Z = 0) = 1 + 2\sum_{K=1}(-1)^K q^{K^2}\cos(2KZ)$ and the total flux at the entrance is the time-dependent Theta function $\theta_3(q = \exp(-D\pi^2 t/L^2, Z = 0) = 1 + 2\sum_{K=1} q^{K^2}\cos(2KZ)$.

Note that the theory can also be formulated for an imposed velocity field. The equation for the steady-state flux leads to $-j_x + j_0 + D_0\partial n/\partial x = 0$. The flux at the entrance of the channel is j_0. The stationary density along the x axis found in this case is $n(x, z) = (j_0 L/D)(1 - x/L)g(z)$.

D. Calculation of efficiency

Of interest for comparison to experiment is the efficiency. The efficiency measures the number of particles which are blocked by the filter. The effect of the system parameters can be examined with the analytical solution.

The average flux $J_x(L, t)$ at the exit gives the number of particles which leave the channel through the yz surface at $x = L$, $J_x(L, t) = \frac{1}{H}\int dz j_x(x = L, z, t)$.

On inserting the expression obtained for the flux,

$$J_x(L,t) = -\frac{kTn_0}{\beta m}\Gamma\frac{\partial f(x = L, t)}{\partial x}. \quad (15)$$

The average flux at the entrance of the channel $J_x(0, t)$ determines the number of particles which enter the channel at $x = 0$ through a cross section perpendicular to the channel axis,

$$J_x(0,t) = -\frac{kTn_0}{\beta m}\frac{\partial f(x = 0, t)}{\partial x}. \quad (16)$$

The function

$$\Gamma = (1/H)\int_0^H dz g(z) \quad (17)$$

measures the number of particles in the channel cross section perpendicular to the channel axis relative to the number at uniform density. The density component $g(z)$ is inserted from Eq. (11) for $\pi^2 Dt/H^2 \gg 1$. Γ is a measure of the permeability κL and stationary permeance [3] $\kappa = J_x/(p(L) - p(0)) = \Gamma/(\beta mL)$.

The stationary density profile corresponds to a time invariant local flux j_x in the direction of the channel and $J_x(L, t) = kTn_0\Gamma/(\beta mL)$. Before entering the membrane the flux is $J_x(0, t) = kTn_0/(\beta mL)$.

The penetration is determined by the ratio of the particle flux leaving the pore to the flux entering the pore,

$$\eta = J_x(L, t)/J_x(0, t). \quad (18)$$

The efficiency is by definition $E = 1 - \eta$.

The calculated efficiency initially decreases in time until reaching the stationary value at times greater than a characteristic time of the order $L^2/\pi^2 D$. The stationary penetration is derived from Eq. (18): $\eta = \Gamma$.

The penetration is essentially the number of particles retained in the channel by interaction with the channel walls and the efficiency is determined by $E = 1 - \Gamma$ for selective rejection or attraction of the particles by the pore.

The number of particles within the pore increases exponentially in temperature through the Boltzmann factors. The efficiency is equal to one in the absence of particles inside the filter or at the exit. The efficiency is large if the repulsive interaction with the filter medium is very large or the temperature low. The efficiency vanishes when the flux at the exit is equal to the flux at the entrance. The efficiency is small if the wall interaction is too weak relative to the thermal energy to cause rejection of particles. The efficiency can be negative for strong wall attraction with increased particle density inside a pore [3].

E. Efficiency increase by cluster formation

An aerosol is composed of solid or liquid particles suspended in air, alone or combined into clusters. Two transport regimes can be identified for transport of nanoparticles in porous media [24]. The first regime is characterized by dominant particle-surface interaction and physicochemical filtration. The second regime is characterized by domination of particle-particle interaction and agglomeration or cluster formation. Here, a cluster is a complex consisting of two or more particles bound together through internal forces. Nanoparticles in suspension are unstable [25,26] with a tendency to form clusters due to strong attractive interparticle interactions (van der Waals, electrostatic, chemical bonding), especially in the presence of repulsive channel walls.

To calculate the effect of cluster formation on the efficiency of filters the coagulation rate is added to the dynamic equation (2) for the number density $n_k(x, z, t)$ of clusters of k particles [6,27]. A solution for the density profile within the channel is proposed:

$$n_k(x, z, t) = f_k(x)g_k(z)h_k(t).$$

The total number density of clusters at a given position is the sum of $n_k(x, z, t)$ over all clusters of size k. The penetration for clusters of size k is

$$\eta_k = \Gamma_k h_k(t)/h_k(0).$$

As in Eq. (17), Γ_k is the amount of k clusters retained in a cross section of the filter. The efficiency for clusters of size k is $E_k = 1 - \eta_k$.

Clusters enter the entrance to the channel at $t = 0$ with a total density $\sum_k n_k(0, z, 0) = n_0$. At time t, $\sum_k n_k(0, z, t) = n_0(t)$. Cluster numbers change with time as small clusters combine into larger clusters during time t before exiting the channel at $x = L$. In a first-order approximation in external

interaction, neglecting the effect of the pressure gradient and the wall potential on aggregation the density profiles along x and z evolve as in previous sections. On separation of variables the equation for the change in the number density with time is the classical coagulation equation [27],

$$dh_k(t)/dt = \omega\left[\sum_{i+j=k} h_i(t)h_j(t) - 2h_k(t)\sum_i h_i(t)\right].$$

The first term on the right describes the formation of k clusters by interaction of i and j clusters with $i + j = k$. The second term describes the loss of k clusters by interaction with all other clusters in the sample. The characteristic time for aggregation is given by $(n_0\omega)^{-1}$. The characteristic time is dependent on the initial concentration of particles and on the strength of the interparticle interaction.

For short times the solution is given for the time dependence of the cluster number density at the entrance with initial concentrations of k-type clusters $h_k(0)$ and total concentration $\sum_i h_I(t) = n_0(t)$

(1) for total number $n_0(t)/n_0 = \frac{1}{1+n_0\omega t}$,

(2) for single particles: $h_1(t)/h_1(0) = \frac{1}{(1+n_0\omega t)^2}$,

(3) for twofold particles: $h_2(t)/h_2(0) = \frac{1}{(1+n_0\omega t)^2} + [h_1(0)^2/h_2(0)n_0]\frac{n_0\omega t}{(1+n_0\omega t)^3}$, and so on.

As an example the initial size distribution for an initially monodisperse sample at the entrance of the channel is $h_1(t = 0)/n_0 = 1$, and $h_k(0) = 0$ for $k > 1$. The calculated retention of single particles is set to $\Gamma_1 = 0.9$. Then at $n_0\omega t = 0.25$ the total number density of clusters has dropped to $n_0(t)/n_0 = 0.8$, and of single particles $h_1(t)/n_0 = 0.64$. The number density of two fold particles clusters $h_2(t)/n_0 = 0.13$. Due to aggregation the apparent efficiency for single particle clusters is increased to $E_1 = 0.42$ for an initially monodisperse sample, while without aggregation $E_1 = 0.1$.

Aggregation continues to affect the number n_k of clusters with time and the apparent efficiency of the smallest particles increases with time as larger and larger clusters form and shift the particle size distribution. For long times the solution of the GDE for the size distribution of aerosols with aggregation can be fit to a log normal distribution with total cluster concentration $N(t)$ at time t, average $\langle\sigma\rangle(t)$ and standard deviation $\sigma_g(t)$ [28]. The penetration is calculated as

$$\eta = \Gamma\left(\frac{N(t)}{N(0)}\right) \times \exp\left\{\frac{\ln\frac{\langle\sigma\rangle(t)}{\langle\sigma\rangle(0)}}{(\ln\sigma_g)^2}\ln\left[\left(\frac{\sigma}{\langle\sigma\rangle(0)}\right)^2\frac{\langle\sigma\rangle(0)}{\langle\sigma\rangle(t)}\right]\right\}. \quad (19)$$

The penetration as a function of particle size can then be expressed as $\eta = A(2\sigma/H)^{2P}$. The resulting efficiency increases with decreasing particle diameter. The proposed relation is consistent with measurements, as in five different filter materials for particle diameters below 100 nm [29].

IV. RESULTS

The efficiency is discussed for simple model potentials of effective molecular interaction between the suspended particles and the molecules of the pore walls. The stationary efficiency is found from the stationary retention Γ. The case of interest is for interaction energy close to the thermal energy and low effective concentration of particles in the suspension, far from the dense packing value for formation of a dense solid phase $1/\sigma^3$. The size of the channel affects particle density inside the channel and the number of particles within the pore.

To validate the theory reliable experiments are needed, but rare, over a large range of pore diameters below 0.1 μm on filter systems with data provided for pore sizes and pore size distribution as well as structure and size distribution of the feed particle system. Numerical simulation could also be used [14,30,31].

Models for the interaction of particles with the pore wall need to be established for each filter system. Forces usually considered are steric repulsion, van der Waals attraction and electrostatic interactions [32,33]. The type of force depends on the chemical structure of the nanoparticles and the complex filter components. The calculated shape of efficiency curve as a function of particle size depends on the type of wall potential for the system. To illustrate results will be given for some simple model potentials and compared with experiments in fibrous filters.

A. Lennard-Jones wall interaction

The Lennard-Jones interaction is a common model used to describe weak interaction between neutral particles. The model potential between the particles and the pore wall is [34]

$$w(z) = \epsilon[2/5(\sigma/z)^{10} - (\sigma/z)^4]. \quad (20)$$

It contains a short-range repulsive interaction due to steric effects and a long-range attraction due to van der Waals forces. For values of $2\sigma/H > 1$ the wall repulsion is smallest at $z = H/2$ and particles will tend to the center of the channel. To obtain an analytical expression for the efficiency and the amount Γ of particles inside the channel an expansion of the effective potential around the minimum at H/2 is inserted into the integral and

$$\eta = \frac{\sqrt{\pi}}{\alpha H}\exp\left(-\frac{2w(H/2)}{kT}\right)erf(\alpha H/2). \quad (21)$$

The curvature α depends on the strength and range of the interaction as well as the channel width, and is of the order of the inverse particle diameter, $\alpha^2 = \frac{1}{kT}\frac{\partial^2 w(H/2)}{\partial z^2}$.

As a result of the saturation of the error function $erf(y) = \frac{2}{\sqrt{\pi}}\int_0^y dse^{-s^2}$, the penetration will tend to zero for large $\alpha H/2$ and the efficiency will be close to one.

For $2\sigma/H < 1$ and increasing channel width the largest particle density lies close to the wall surfaces due to the van der Waals attraction [3]. The integral for Γ is calculated as the sum in a Taylor expansion on the two minima of the wall interaction at $z = z_c$, a distance of the order of the particle diameter σ and $z = H - z_c$. The curvature parameter α_c at $z = z_c$ is $\alpha_c^2 = \frac{1}{2kT}\frac{\partial^2 w(z_c)}{\partial z^2}$. For large pores, the penetration is

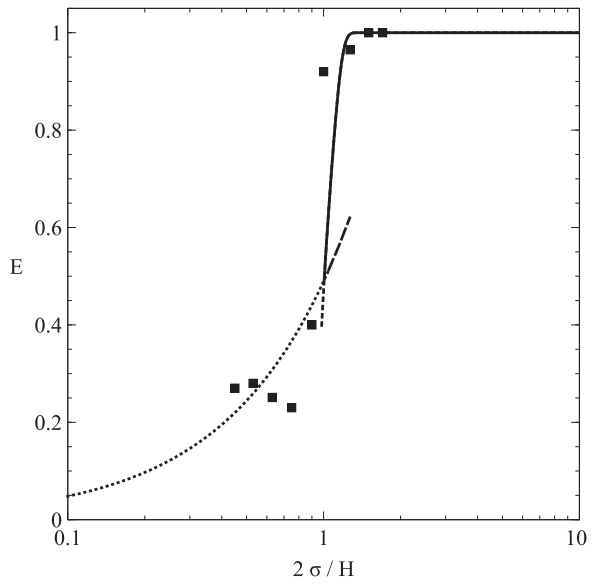

FIG. 2. The efficiency E as a function of $2\sigma/H$ (particle diameter σ to channel width H) using the solution in wide pores for $\sigma/H \to 0(\cdots)$ and in narrow pores for $\sigma/H \gg 1(-)$. The Lennard-Jones wall interaction parameter is $\epsilon/kT = 0.8$. The tungsten oxide nanoparticle filter efficiency measured in the nanofibrous polyvinylalcohol filter F5 from Fig. 4 in Ref. [31] is shown for comparison (■) for an effective channel width $H = 4$ nm.

then

$$\eta = \frac{\sqrt{\pi}}{\alpha_c H} \exp\left(\frac{-w(z_c)}{kT}\right) erf(\alpha_c z_c) + \frac{(H - 2z_c)}{H}. \quad (22)$$

The efficiency E is shown in Fig. 2 as a function of $2\sigma/H$ for the steady state. In narrow channels, the overlap of the short-range repulsion dominates with a minimum value at the center. Large particles are impeded from entering, the density is small and the efficiency for large $2\sigma/H$ is close to one with significant rejection of particles. Rejection of particles by the size effect is one way to produce high efficiency. The efficiency can be close to one over a large range of particle size if the effective pore size is small, smaller than the smallest particle diameter. When the channel width and the particle diameter are similar the well at the center of the channel is lower leading to increase of density at the middle of the channel and a decrease in efficiency for a pore width close to twice the particle diameter.

As the pore size increases, the effective wall interaction is attractive. More particles are attracted into and exit from the channel further decreasing the efficiency. The mechanism which produces greater penetration is the attraction of the pore walls (which in equilibrium causes adsorption in the channel for large values of ϵ/kT). For smaller $2\sigma/H$ the effect of the wall interaction is weaker and limited to a zone close to the pore surface; particles can pass through the channel and exit with little change of the number density. The efficiency decreases toward zero. Experimental efficiency curves have been reported which indicate low efficiency for small particles (called thermal rebound) and the need for a theoretical basis [9,35,36].

As an example, the steady-state efficiency is shown for WO_2 nanoparticles for the size range of 0.82 to 3.3 nm diameter in Polyvinyl alcohol nanofibrous filters [37]. These materials are dominated by covalent bonding and a Lennard-Jones-type interaction between particles and walls would be a reasonable choice. Inorganic materials can form nanocrystals; however, tungsten oxide clusters are expected to be correctly modeled as spheres for small diameters. In the experiment the efficiency of a set of filters with different fiber structure was measured. The fibrous filters were prepared under different conditions of electrospinning. In all six filters of the experiment the measured efficiency shows a rapid decrease around a particle diameter of 2 nm with the long tail typical of the effect of an attractive well for pore diameters greater than twice the particle diameter. The effective pore width would be around 4 nm to fit the theory. Due to the random nature of electrospinning the characteristics and performance of the filters of the experiment differ. The presence of large pores in a bimodal pore size distribution lowers the average efficiency. For example in the lower weight filter F4 the efficiency goes from 0.8 at $2\sigma/H > 1$ to below 0.1 for $2\sigma/H < 1$.

B. Soft sphere wall interaction

The simple and mathematically convenient family of potentials which model repulsive cores are the soft sphere potentials: $\epsilon_0(\sigma/r)^p$. The average interaction in the z- direction of a particle with a wall of charge density ρ is

$$w(z) = 2\pi\rho\epsilon_0 \int_0^\infty dXX \int_{-\infty}^{-z} dZ \frac{\sigma^p}{(\sqrt{X^2 + Z^2})^p}, \quad (23)$$

which can be written $w(z) = \epsilon(\sigma/z)^{p-3}$.

Two models will be considered for the average interaction with the wall: $w(z) = \epsilon(\sigma/z)$ with $p = 4$ and wall interaction $w(z) = \epsilon(\sigma/z)^3$ for $p = 6$. A complete physical justification for soft sphere repulsion is lacking [38]. In an electrostatic multipole expansion [39] a charge interacting with an octupole or a dipole with a quadrupole corresponds to $p = 4$. Octupole-quadrupole or dipole-hexadecapole terms correspond to $p = 6$.

The pore wall interaction for $w(z) = \epsilon(\sigma/z)$ and the resulting density profile across the width of the pore channel are shown in Fig. 3 for a channel of a width of four times the particle diameter. The density is lower within the channel due to the repulsive wall potential. The repulsive interactions of each of the walls overlap, the wall interaction has a minimum at $z = H/2$ and particles will tend to the center of the channel. The repulsion at the center of the pore is stronger the smaller the channel width.

The time dependence of the efficiency calculated from Eq. (14) inserted in Eqs. (15) and (16) is shown in Fig. 4. The efficiency decreases with time until reaching the stationary value. The penetration varies from zero at $t = 0$ to the stationary value of Γ at $t = \infty$. Smaller particles reach the stationary value faster than larger ones. The dependence on time is measured by the characteristic time $L^2/\pi^2 D$ and persists longer the smaller the diffusion coefficient. The diffusion coefficient depends on particle size with an increase for small particles as described for example by the macroscopic Stokes Einstein equation [40]. Time dependence persists longer for larger

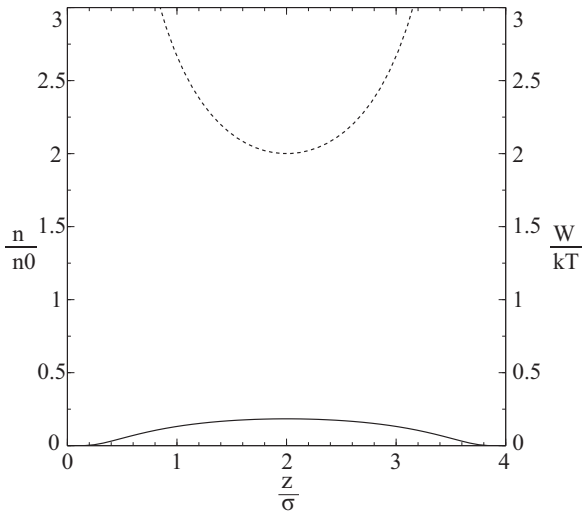

FIG. 3. The interaction $W(z)/kT(\cdots)$ of the channel wall with suspended particles of diameter σ and the local suspended particle density profile $n(z)/n_0(-)$ along the width ($H = 4\sigma$) of the channel at the entrance of the channel for wall interaction $w(z) = \epsilon(\sigma/z)$ with $\epsilon/kT = 2$. The density of particles before entering the channel is n_0.

particles with possible overlap of stationary and nonstationary states in polydisperse mixtures.

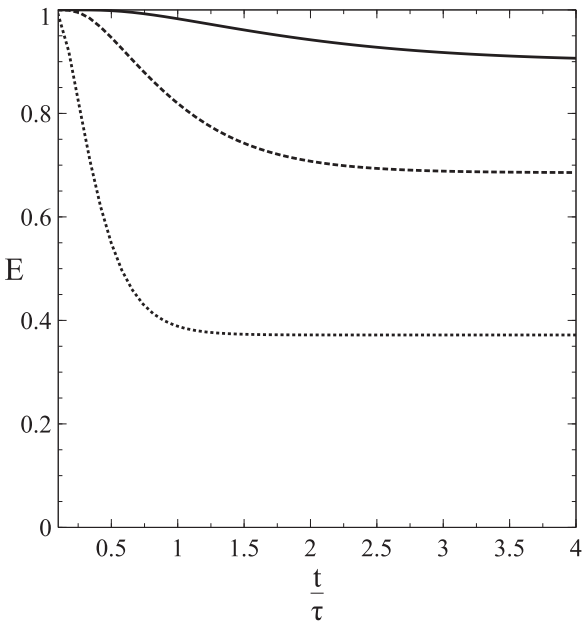

FIG. 4. The efficiency E for a channel of length L as a function of time t/τ for three values of particle size $\sigma(-)$, $\sigma/2(--)$, $\sigma/5(\cdots)$ corresponding to three values of characteristic time τ, $\tau/2$, $\tau/5$ of decreasing particle size. The characteristic time $\tau = L^2/(\pi^2 D)$ is determined by the size dependent diffusion coefficient D, 2D, 5D of the suspended particles in the channel. Steady-state efficiency is taken from Fig. 5 for $w(z) = \epsilon(\sigma/z)$ at $(2\sigma/H) = 0.5$

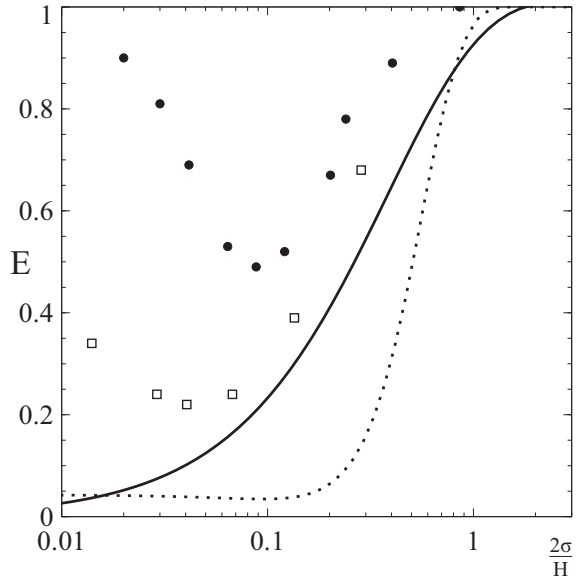

FIG. 5. The efficiency E as a function of $(2\sigma/H)$ for repulsive wall potential $\epsilon(\sigma/z)$ (–) and $\epsilon(\sigma/z)^3$ $(\cdots)$. The channel width is H, the particle diameter is σ and $\epsilon/kT = 1$. The efficiency measured for NaCl aerosol particles in polycarbonate filters in Fig. 4 of Ref. [31] are shown for channel widths $H = 1\mu(\bullet)$ and $H = 3\mu(\square)$.

The steady-state penetration η is calculated from Eq. (21) for the model potential $\epsilon(\sigma/z)$ as a function of $Q = 2\sigma/H$,

$$\eta = \frac{\sqrt{\pi}}{2}\frac{1}{\sqrt{2Q\epsilon/kT}} erf(\sqrt{2Q\epsilon/kT}) e^{-(2Q\epsilon/kT)},$$

and for $\epsilon(\sigma/z)^3$,

$$\eta = \frac{\sqrt{\pi}}{2}\frac{1}{2\sqrt{3Q^3\epsilon/kT}} erf(2\sqrt{3Q^3\epsilon/kT}) e^{-(2Q^3\epsilon/kT)}.$$

Due to the saturation of error function, the penetration will be close to zero for $Q > 4$ and the efficiency will be large, close to one.

The calculated efficiency is shown in Fig. 5 for the soft sphere potentials and a moderate interaction strength $\epsilon/kT = 1$. The short-range repulsion $\epsilon(\sigma/z)^{p-3}$ hinders entry of particles into the pore. The penetration is small and less than 0.1 for $2\sigma/H > 1$. Large particles penetrate less than smaller particles as expected due to the size effect. For larger pore width the repulsive interaction is effective only close to the walls and the efficiency decreases. As the particle size decreases to zero the theoretical penetration rapidly goes to one and the efficiency decreases to zero. The decrease is slower for the longer range interaction in $1/z$. Similar results are obtained for hard spheres with attractive interaction $-\epsilon(\sigma/z)^p$; corresponding to ion-polarizable molecule interaction for $p = 4$ and to neutral molecules for $p = 6$.

In many aerosol filters the measured efficiency as a function of particle size follows a more or less shallow U-curve, with an increase, not found in the present calculation for decreasing particle diameter below 0.1 μm.

The steady-state efficiency $E = 1 - \eta$ measured [41] for NaCl aerosols with particle diameters between 10 and 500 nm in polycarbonate filters is given in Fig. 5. The filter structure is regular with pore widths of 1 and 3 μm. For particle

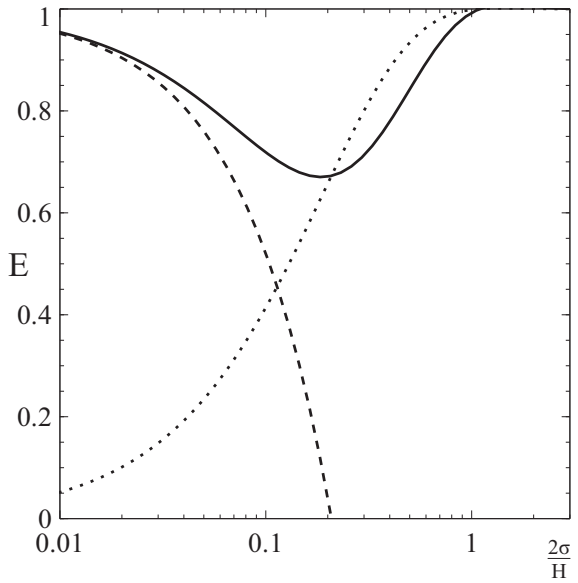

FIG. 6. The efficiency E as a function of $(2\sigma/H)$ due to formation of clusters $(--)$, due to repulsive wall interaction $(\cdots)$, and total apparent efficiency (–). Channel width is H, particle diameter is σ.

sizes $2\sigma/H > 0.1$ the experiment can be fit to the theoretical curve in the one micron filter using a dominant wall interaction $w(z) = \epsilon(\sigma/z)$. Below the particle diameter of 50 nm the experimental efficiency increases again as predicted in the conventional theory of filtration by increased diffusion, whereas in the present kinetic theory the calculated efficiency continues to decrease to zero. Evidence of agglomeration has been reported in a 2 μm polycarbonate filter for NaCl nanoparticles of diameter between 10 and 100 nm [29]. Aggregation of small particles into clusters [6,42] results in loss of the smallest particle sizes with apparent increase in efficiency.

To illustrate the efficiency from Eq. (19) for cluster formation alone is plotted in Fig. 6 for a reasonable choice of parameters [43]: $\Gamma = 1$, constant $\sigma_g = 2$ and (measured) $\langle\sigma\rangle(0) = 0.18$ μm, $\langle\sigma\rangle(t)/\langle\sigma\rangle(0) = 1.3$, $N(t)/N(0) = 1$. Then $\eta = 4.8(2\sigma/H)$. The efficiency due to repulsive walls with interaction $w(z) = \epsilon(\sigma/z)$ is also plotted in Fig. 6 for $\epsilon/kT = 2$ as well as the total combined efficiency.

Cluster formation within the pore channel in generated aerosol samples leads to an apparent loss of the smallest particles and measured increase of efficiency for small particle size. The effect depends on the evolution of the initial aerosol size distribution and is enhanced by strong forces between particles, in particular electrostatic interactions between cluster charge distributions. The question justifies further experimental and theoretical investigation.

V. CONCLUSIONS

Some straightforward observations already highlighted elsewhere [44] are supported by the present study. Based on the results of the model presented the best filters with high efficiency over a large range of particle dimensions would require:

(1) Pore width smaller than twice the smallest diameter of the suspended nanoparticles for filtration by size exclusion. Below this value the efficiency is close to one as was shown for the model potentials. For example fabric filter materials with tight weaves and small pore sizes are preferable.

(2) Strong repulsive interaction relative to the thermal energy to hinder the nanoparticles from entering the pore. The penetration was given as an exponential function of the wall potential and the slope of the efficiency with particle size reflects the variation of the potential with distance. Aerosols often appear to be charged and this could be exploited to enhance efficiency. Electrostatic filtering of aerosols is well documented and continues to be explored [45]. Certain materials such as silk provide good electrostatic filtering by their chemical structure.

(3) Large pore lengths, possibly by layering, to slow decay to the stationary state of lower efficiency within the characteristic time which varies as L^2. Combining layers has also been suggested for optimal wearability and breathability in masks.

VI. DISCUSSION

Examining how nanoparticles move through porous media contributes to current theories of nanoparticle transport and diffusion [40,46,47]. The present approach considers flow in a pressure gradient with Brownian motion for particles in the force field of the channel walls, employing potentials of mean force in a simple model pore structure and including aggregation into clusters. The model is useful to understand filtration of particles in filters and membranes on the nanoscale.

Stochastic kinetic theories of matter have been successfully applied to a number of mesoscopic systems: dilute molecular gases, high molecular weight polymer solutions and melts, as well as micrometer sized colloids and suspensions often used as models for molecular systems. The aerosols studied here are sufficiently dilute and limited in size to justify the validity of the approach.

Extension to other geometries [19] and other model potentials with attractive and repulsive contributions as well as to more complex systems such as virus filtration [48,49] is straightforward. Combining knowledge of molecular structure with a probability based transport theory is a useful multiscale approach in materials where long time constants make computational methods difficult.

[1] H. Strathman, Membrane separation processes: Current relevance and future opportunities, AIChE J. **47**, 1077 (2001).

[2] S. P. Adiga, C. Jin, L. A. Curtiss, N. A. Monteiro-Riviere, and R. J. Narayan, Nanoporous membranes for medical and biological applications, Wiley Interdisc. Rev.: Nanomed. Nanobiotechnol. **1**, 568 (2009).

[3] A. ten Bosch, Kinetic theory of gas separation in a nanopore and comparison to molecular dynamics simulation, J. Chem. Phys. **122**, 084711 (2005).

[4] A. Tcharkhtchi, N. Abbasnezhad, M. Z. Seydani, N. Zirak, S. Farzaneh, and M. Shirinbayan, An overview of filtration efficiency through the masks: Mechanisms of the aerosols penetration, Bioact. Mater. **6**, 106 (2021).

[5] J. Wang and P. Tronville, Toward standardized test methods to determine the effectiveness of filtration media against airborne nanoparticles, J. Nanopart. Res. **16**, 2417 (2014).

[6] S. K. Friedlander *et al.*, *Smoke, Dust, and Haze*, Vol. 198 (Oxford University Press, New York, NY, 2000).

[7] W. C. Hinds, *Aerosol Technology: Properties, Behavior, and Measurement of Airborne Particles* (John Wiley & Sons, New York, NY, 1999).

[8] G. Boccardo, T. Tosco, A. Fujisaki, F. Messina, A. Raoof, D. R. Aguilera, E. Crevacore, D. L. Marchisio, and R. Sethi, A review of transport of nanoparticles in porous media: From pore-to macroscale using computational methods, in *Nanomaterials for the Detection and Removal of Wastewater Pollutants* (Elsevier, 2020), Chap. 13, pp. 351–381.

[9] R. Givehchi, Z. Tan *et al.*, An overview of airborne nanoparticle filtration and thermal rebound theory, Aeros. Air Qual. Res. **14**, 46 (2014).

[10] F. Miele, P. de Anna, and M. Dentz, Stochastic model for filtration by porous materials, Phys. Rev. Fluids **4**, 094101 (2019).

[11] S. K. Friedlander and D. Y. Pui, Emerging issues in nanoparticle aerosol science and technology, J. Nanopart. Res. **6**, 313 (2004).

[12] C. M. Sorensen, R. C. Flagan, U. Baltensperger, and D. Y. Pui, Grand challenges for aerosol science and technology, Aeros. Sci. Technol. **53**, 731 (2019).

[13] Z. Pan, Y. Liang, M. Tang, Z. Sun, J. Hu, and J. Wang, Simulation of performance of fibrous filter media composed of cellulose and synthetic fibers, Cellulose **26**, 7051 (2019).

[14] A. Phan, D. Fan, and A. Striolo, Fluid transport through heterogeneous pore matrices: Multiscale simulation approaches, Phys. Fluids **32**, 101301 (2020).

[15] I. R. de Anda, J. W. Wilkins, J. F. Robinson, C. P. Royall, and R. P. Sear, Modeling the filtration efficiency of a woven fabric: The role of multiple lengthscales, Phys. Fluids **34**, 033301 (2022).

[16] A. ten Bosch, Kinetic path to fluid dynamics in membranes, MRS Online Proc. Library **752**, 79 (2002).

[17] J. F. Morris, Toward a fluid mechanics of suspensions, Phys. Rev. Fluids **5**, 110519 (2020).

[18] P. Klobes, M. Klaus, and R. Munro, Porosity and specific surface area measurements for solid materials, Inst. Stand. Technol. Special Pub. **1** (2006).

[19] A. ten Bosch, A model for nanopore gas permeation, Sep. Purif. Technol. **47**, 156 (2006).

[20] A. ten Bosch, *Analytical Molecular Dynamics of Fluids: From Atoms to Oceans* (ten Bosch, 2019).

[21] J. H. Seinfeld and S. N. Pandis, *Atmospheric Chemistry and Physics: From Air Pollution to Climate Change* (John Wiley & Sons, Inc., New York, NY, 2006).

[22] F. Gelbard and J. H. Seinfeld, The general dynamic equation for aerosols: Theory and application to aerosol formation and growth, J. Colloid Interface Sci. **68**, 363 (1979).

[23] S. Qiu and M. Vuorinen, Special functions in geometric function theory, Handbook of complex analysis, Geomet. Funct. Theory **2**, 621 (2005).

[24] P. Babakhani, J. Bridge, R.-a. Doong, and T. Phenrat, Continuum-based models and concepts for the transport of nanoparticles in saturated porous media: A state-of-the-science review, Adv. Colloid Interface Sci. **246**, 75 (2017).

[25] E. R. Whitby and P. H. McMurry, Modal aerosol dynamics modeling, Aerosol Sci. Technol. **27**, 673 (1997).

[26] L. Marks and L. Peng, Nanoparticle shape, thermodynamics and kinetics, J. Phys.: Condens. Matter **28**, 053001 (2016).

[27] S. Chandrasekhar, Stochastic problems in physics and astronomy, Rev. Mod. Phys. **15**, 1 (1943).

[28] Z. Xu and B. Zhou, *Fundamentals of Air Cleaning Technology and Its Application in Cleanrooms* (Springer, Berlin, 2014).

[29] J.-C. Soo, K. Monaghan, T. Lee, M. Kashon, and M. Harper, Air sampling filtration media: Collection efficiency for respirable size-selective sampling, Aeros. Sci. Technol. **50**, 76 (2016).

[30] N. A. Marrufo-Hernández, M. Hernández-Guerrero, J. M. Nápoles-Duarte, J. P. Palomares-Báez, and M. A. Chávez-Rojo, Prediction of the filtrate particle size distribution from the pore size distribution in membrane filtration: Numerical correlations from computer simulations, AIP Adv. **8**, 035308 (2018).

[31] A. Boţan, F.-J. Ulm, Roland J.-M. Pellenq, and B. Coasne, Bottom-up model of adsorption and transport in multiscale porous media, Phys. Rev. E **91**, 032133 (2015).

[32] J. N. Israelachvili, *Intermolecular and Surface Forces* (Academic Press, San Diego, CA, 2011).

[33] G. Karlstrom and B. Jonsson, Intermolecular interactions, Lecture notes, Dept. Theoretical Chemistry, Lund University (2013), https://www.teokem.lu.se/fileadmin/teokem/ms6.pdf.

[34] D. W. Siderius and L. D. Gelb, Extension of the Steele 10-4-3 potential for adsorption calculations in cylindrical, spherical, and other pore geometries, J. Chem. Phys. **135**, 084703 (2011).

[35] W. J. Kowalski and W. P. Bahnfleth, Merv filter models for aerobiological applications, Air media **2002**, 13 (2002).

[36] P. C. Raynor and S. J. Chae, The long-term performance of electrically charged filters in a ventilation system, J. Occup. Environ. Hyg. **1**, 463 (2004).

[37] R. Givehchi, Q. Li, and Z. Tan, Filtration of sub-3.3-nm tungsten oxide particles using nanofibrous filters, Materials **11**, 1277 (2018).

[38] J. A. Rackers and J. W. Ponder, Classical pauli repulsion: An anisotropic, atomic multipole model, J. Chem. Phys. **150**, 084104 (2019).

[39] J. A. Te, An approximate multipole expansion for molecular interactions, Ph.D. thesis, Georgetown University, 2010.

[40] K. A. Rose, M. Molaei, M. J. Boyle, D. Lee, J. C. Crocker, and R. J. Composto, Particle tracking of nanoparticles in soft matter, J. Appl. Phys. **127**, 191101 (2020).

[41] N. C. Burton, S. A. Grinshpun, and T. Reponen, Physical collection efficiency of filter materials for bacteria and viruses, Ann. Occupat. Hygiene **51**, 143 (2007).

[42] B. R. Bzdek and J. P. Reid, Perspective: Aerosol microphysics: From molecules to the chemical physics of aerosols, J. Chem. Phys. **147**, 220901 (2017).

[43] M. Olin, T. Anttila, and M. Dal Maso, Using a combined power law and log-normal distribution model to simulate particle

formation and growth in a mobile aerosol chamber, Atmos. Chem. Phys. **16**, 7067 (2016).

[44] A. Konda, A. Prakash, G. A. Moss, M. Schmoldt, G. D. Grant, and S. Guha, Aerosol filtration efficiency of common fabrics used in respiratory cloth masks, ACS Nano **14**, 6339 (2020).

[45] A. L. Sanchez, J. A. Hubbard, J. G. Dellinger, and B. L. Servantes, Experimental study of electrostatic aerosol filtration at moderate filter face velocity, Aerosol Sci. Technol. **47**, 606 (2013).

[46] D. M. Tartakovsky and M. Dentz, Diffusion in porous media: Phenomena and mechanisms, Transp. Porous Media **130**, 105 (2019).

[47] A. Vilquin, V. Bertin, P. Soulard, G. Guyard, E. Raphaël, F. Restagno, T. Salez, and J. D. McGraw, Time dependence of advection-diffusion coupling for nanoparticle ensembles, Phys. Rev. Fluids **6**, 064201 (2021).

[48] A. Armanious, M. Aeppli, R. Jacak, D. Refardt, T. Sigstam, T. Kohn, and M. Sander, Viruses at solid–water interfaces: A systematic assessment of interactions driving adsorption, Environ. Sci. Technol. **50**, 732 (2016).

[49] O. Harriman and M. Leake, Single molecule experimentation in biological physics: Exploring the living component of soft condensed matter one molecule at a time, J. Phys.: Condens. Matter **23**, 503101 (2011).